Journal of the Serbian Chemical Society
JSCS@tmf.bg.ac.rs • www.shd.org.rs/JSCS
J. Serb. Chem. Soc. *88* (4) 423–435 (2023)
JSCS–5636
Original scientific paper
Published 26 March 2023

Performance of carbon-coated magnetic nanocomposite in methylene blue and arsenate treatment from aqueous solution

NGOC BICH NGUYEN[1,2]*, THI QUE PHUONG PHAN[3], CAO THANH TUNG PHAM[1,4], HUU NGHI NGUYEN[2], SY NGUYEN PHAM[5], QUOC KHUONG ANH NGUYEN[6]** and DINH THANH NGUYEN[1,3]***

[1]Graduate University of Science and Technology, Viet Nam Academy of Science and Technology, Hanoi City, 100000, Vietnam, [2]Dong Thap University, Cao Lanh City, 870000, Vietnam, [3]Institute of Applied Materials Science, Viet Nam Academy of Science and Technology, Ho Chi Minh City, 700000, Vietnam, [4]Institute of Chemical Technology, Viet Nam Academy of Science and Technology, Ho Chi Minh City, 700000, Vietnam, [5]Ho Chi Minh City University of Natural Resources and Environment, Vietnam and [6]Institute of Applied Technology and Sustainable Development, Nguyen Tat Thanh University, Ho Chi Minh City, 70000, Vietnam

(Received 2 August, revised 5 October, accepted 3 November 2022)

Abstract: Herein, carbon-coated magnetic nanocomposite fabricated by a low-temperature hydrothermal method was used for methylene blue and arsenate treatment in aqueous solution. The Langmuir model fits the experimental data with a calculated maximum adsorption capacity of 110.63 and 2.31 mg g^{-1} for methylene blue and arsenate adsorption, respectively. Furthermore, the adsorption mechanisms of methylene blue as well as arsenate are physical adsorption and a combination of physical adsorption and chemisorption, respectively. Gibbs energy change with negative values indicates that methylene blue and arsenate adsorption on magnetic materials occurs naturally. This research demonstrated a simple, efficient, and reliable method for removing methylene blue and arsenate.

Keywords: hydrothermal carbonization; rice straw; adsorption.

INTRODUCTION

The rapid development of industries has posed many potentially serious issues in relation to ecosystems such as heavy metal and dye contamination.[1] Several technologies have been introduced for wastewater treatment, including oxidation, photocatalytic degradation, ultrafiltration, adsorption/precipitation process and coagulation.[2] Adsorption has been regarded as one of the most common

* Corresponding authors. E-mail: (*)nnbich@dthu.edu.vn; (**)nqkanh@ntt.edu.vn; (***)dinhthanhng53@gmail.com
https://doi.org/10.2298/JSC220802080N

Available on line at www.shd.org.rs/JSCS/
(CC) 2023 SCS.

and effective techniques for contaminant removal from wastewater.[3] Recently, carbon material derived from low-cost biomass residuals such as rice straw has received a lot of attention due to its potential environmental benefits.[4] Moreover, magnetic modifications of the low-cost adsorbents can result in novel adsorbents that can be rapidly removed from the treated solution using a magnetic separator.[5]

Methylene blue (MB) is used in many fields, so a significant amount of MB ends up in wastewater, posing a risk to aquatic life. In addition, due to its high toxicity, arsenic can cause serious health problems such as lung, liver, kidney, and skin cancers.[6–11] As a result, it is critical to investigate efficient technologies for extracting MB and As(V) from aqueous solutions.[12–16] Rice straw (RS) is an inexpensive and abundant carbon-containing lignocellulose in Vietnam. In the paper industry, biomass is usually pre-alkali-treated to remove lignin. As a result, this process emits a large amount of black liquor containing lignin, which can be utilized for carbon-containing materials.[17]

In this study, we simultaneously carbonize and magnetize the lignin liquor obtained from rice straw to synthesize carbon-coated magnetic nanocomposite (CMC) by a hydrothermal method. The primary goal of this work is to study the potential adsorption of low-cost CMC for MB and As(V) from wastewater. Aside from that, another goal is to evaluate the effect of concentration, contact time, temperature and pH solution. This work also discusses the Langmuir and Freundlich adsorption isotherm models, as well as various thermodynamic parameters like change in heat of adsorption (ΔH^{o}), entropy change (ΔS^{o}) and Gibbs energy change (ΔG^{o}) in MB and As(V) adsorption.

EXPERIMENTAL

Materials

RS was collected in Vietnam and washed several times with distilled water before being milled into powder and filtered through a 250-mesh sieve.

Potassium hydroxide (KOH, ≥ 85 %), sodium hydroxide (NaOH, ≥ 97 %), hydrochloric acid (HCl, 37 %), iron(III) nitrate nonahydrate ($Fe(NO_3)_3$ $9H_2O$, ≥ 99 %), sodium chloride (NaCl, ≥ 99.5 %), H_3AsO_4 in HNO_3 0.5 mol L^{-1} 1000 mg L^{-1} purchased from Merck. MB ($C_{16}H_{18}N_3SCl{\cdot}H_2O$, 99.5 %), was obtained from Sigma–Aldrich. All chemicals used were of analytical grade and were used as received without any further purification.

Synthesis of carbon-coated magnetic nanocomposite

Firstly, 15 g of RS was combined with 150 ml KOH 5 %. The mixture was hydrothermally treated in an autoclave at 120 °C for 4 h. After slowly mixing 50 ml of 0.125 mol $Fe(NO_3)_3$ into 125 ml of the above-solution for 2 h, hydrothermal treatment was carried out at 180 °C for 14 h. The CMC is then collected by filtration and rinsed several times with distilled water until the pH value reached neutral. Finally, the remaining solid was dried in an oven at 40 °C for 12 h. In comparison, a blank sample (BS) was fabricated under the same condition but without the addition of $Fe(NO_3)_3$.

(CC) 2023 SCS.

Characterization of CMC

X-ray diffraction (XRD) was carried out ON X D8 Advance Bruker with CuK_α radiation (λ = 0,15418 nm). The morphology was observed with S4800 Hitachi scanning electron microscope (SEM) and JEM1400 JEOL transmission electron microscopy (TEM). Energy-dispersive X-ray spectrum (EDS) was recorded on H7593 Horiba. The Fourier transform infrared (FT-IR) spectroscopy was measured on IR Affinity-1S spectrophotometer (Shimadzu). The specific surface area (BET) was determined by N_2 adsorption–desorption isotherms at liquid nitrogen temperature (77 K) using Quantachrome TriStar 3000 V6.07A adsorption instruments. Magnetization measurements were carried out using a vibrating sample magnetometer (VSM) 7307, Lake Shore, USA. The UV–Vis spectrometry was recorded on Spectro UV--2650, Labomed, USA, at a wavelength of 664 nm. Residual As(V) was detected by Thermo Scientific iCAP Q ICP–MS. The point of zero charge (pH_{PZC}) of CMC was investigated by the solid addition method.[18] A series of 45 mL of 0.5 M NaCl solutions were prepared in 100 mL flasks. The initial pH value (pH_i) of the solution was adjusted from 2 to 12 using either 0.1 M NaOH or 0.1 M HCl solutions. The total volume of solution in each flask was precisely 50 mL by adding distilled water. Then, 0.1 g of CMC was added to each flask and kept on shaker at 180 rpm for 24 h. The final pH (pH_f) of the solutions was recorded. The difference between the initial and final pH ($\Delta pH = pH_i - pH_f$) was plotted against pH_i. The point of intersection of the curve with the abscissa, where $\Delta pH = 0$, presented pH_{PZC}.

Adsorption experiment

Adsorption experiments were carried out using 0.1 g CMC in 100 mL of solution. Variable parameters including initial concentration, contact time, temperature, and pH of the medium were thoroughly investigated. The initial pH value of the solution was adjusted using either 0.1 M NaOH or 0.1 M HCl solutions. All adsorption experiments were carried out in duplicate. At predetermined time intervals, the adsorbent and solution were separated, and the residual MB and As(V) concentrations in the solution were measured using UV–Vis and ICP––MS, respectively.

The removal rate, R / %, was calculated as:

$$R = 100(C_0 - C_e)/C_0 \quad (1)$$

where C_0 and C_e are the initial and equilibrium concentrations of MB or As(V) solution. We listed different kinetic models, thermodynamic equations, and adsorption isotherms in Table S-I of the Supplementary material to this paper.

Non-linear chi-square test

Optimization is indispensable in order to identify the suitable kinetic and isotherm models to the obtained experimental results. For the present study, apart from correlation coefficient (R^2), a non–linear regression model is chi–square test was performed for data optimization process. The chi–square (χ^2) can be expressed as equation (2):

$$\chi^2 = \Sigma \frac{\left(q_{e,exp} - q_{e,cal}\right)^2}{q_{e,cal}} \quad (2)$$

where $q_{e,exp}$ is the experimental value of adsorption capacity and $q_{e,cal}$ is the calculated value from the model. If experimental data is analogous to that from the model, χ^2 will be small, otherwise, it will be large.

(CC) 2023 SCS.

Reusability

0.1 g CMC was added to 100 mL of a solution (120 mg L^{-1} for MB and 2.5 mg L^{-1} for As(V) and stirred for 60 and 90 min, respectively, for saturated adsorption. Following the magnetic separation, the supernatant solution was discarded, and only adsorbed CMC was collected. The adsorbed CMC in the case of MB was then added to ethanol and a 0.1 M HCl solution in the case of As(V) for the desorption process.[13,14] The experiments were repeated 5 times in sequence to estimate the potentially regenerable property of CMC.

RESULTS AND DISCUSSION

Characterization of materials

As shown in Fig. 1a, regarding BS, the broad peak at 2θ = 22° represented the characteristic reflection of carbon.[19] In CMC, the diffractions at 2θ 30.46, 35.86, 43.58, 57.25 and 62.65° correspond to crystalline magnetite Fe_3O_4 (JCPDS No. 19-0629), which agree with the literature data.[20] This demonstrated that Fe(III) is reduced into Fe_3O_4 by carbon, which is formed under hydrothermal conditions by the reactions (3)–(6):[2]

$$FeCl_3 + 3KOH \rightarrow Fe(OH)_3 + 3KCl \quad (3)$$

$$Fe(OH)_3 \rightarrow FeOOH + H_2O \quad (4)$$

$$2FeOOH \rightarrow Fe_2O_3 + H_2O \quad (5)$$

$$2Fe_2O_3 + C \rightarrow 2Fe_3O_4 + CO \quad (6)$$

In Fig. 1b, FT-IR spectra revealed that both BS and CMC contained functional groups at 3413–3422 cm^{-1} (–OH stretching vibrations), 1627–1630 cm^{-1} (C=O stretching vibration), 1110–1114 cm^{-1} (C–O stretching vibration), 799––818 cm^{-1} and 450–474 cm^{-1} (Si–O–Si stretching vibration) and 1451–1456 cm^{-1} (–O–CH_3 deformation vibration).[1,18,20] In general, the intensity of all peaks in CMC is lower than that of BS and has a slight shift, indicating that chemical reactions occurred when Fe^{3+} was added to the solution. The peak near 560 cm^{-1}, assigned to the Fe–O stretching vibration, was only visible in CMC, which is consistent with XRD result.[12]

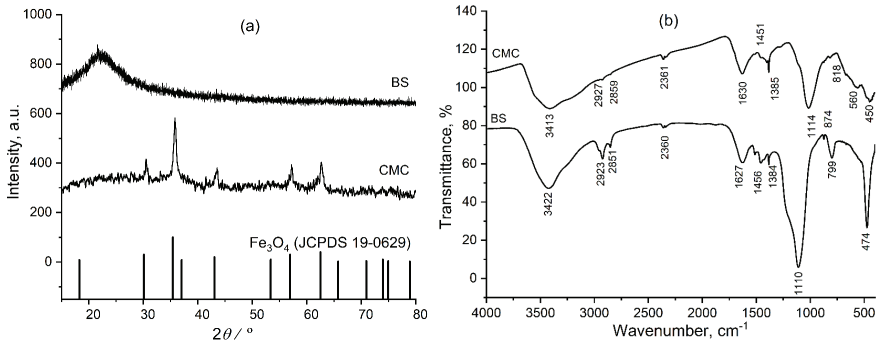

Fig. 1. a) XRD patterns of BS, CMC and standard Fe_3O_4 (JCPDS No. 19-0629); b) FT-IR spectra of BS and CMC.

(CC) 2023 SCS.

According to Figs. S-1 and S-2 of the Supplementary material, CMC is made up of C (19.21 %), O (34.38 %), Fe (42.24 %) and Si (4.16 %). In addition, EDS elemental mapping also shows that Fe is uniformly dispersed on the surface of the material, proving that iron oxide was formed in CMC. Fig. 2a and b depicts typical TEM and SEM images of CMC containing Fe_3O_4 with sizes ranging from 50 to 120 nm and carbon as a shell with a thickness ranging from 30 to 50 nm. At room temperature, Fig. S-3 shows the saturation magnetisation value of 33.7 emu g^{-1}, which allows for the rapid separation and redistribution of CMC from aqueous solution and leads to cost-effective and reusable applications.[21] Table S-II compares the magnetization of CMC with various biochar.

Table S-III displayed specific surface area, total pore volume, and mean pore size for RS, BS, and CMC. The specific surface area of CMC (171.4 m^2 g^{-1}) is significantly greater than that of BS (6.6 m^2 g^{-1}) thanks to the combination of carbon and magnetic particles.[22] Furthermore, the mean pore size of CMC (6 nm) is smaller than that of BS (33 nm), attributed to the covered micropores in carbon.[23]

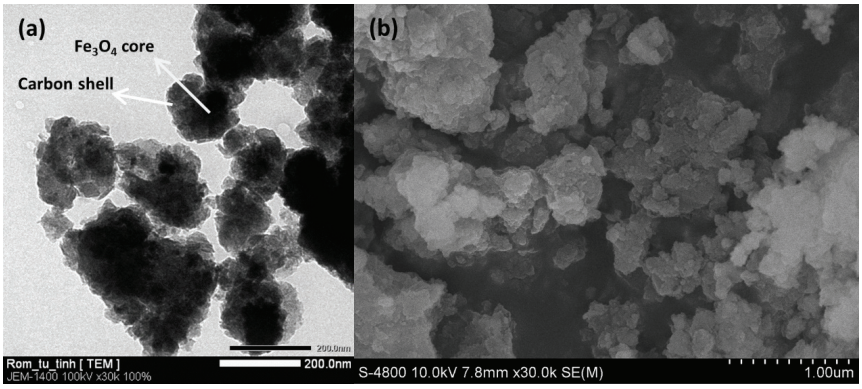

Fig. 2. TEM (a) and SEM (b) images of CMC.

Effect of initial solution pH

The pH of the solution plays an important role in the adsorption process, particularly in terms of adsorption capacity.[24] Because of the changing surface of CMC on MB and As(V), the pH value can alter its performance.[25] Investigation on the influence of initial pH solutions from 3 to 11 was carried out while keeping other parameters constant such as initial concentration (120 and 2.5 mg L^{-1}), equilibrium time (60 and 90 min at 303 K) for MB and As(V), respectively. The effect of pH on the adsorption of MB and As(V) on CMC is depicted in Fig. 3a and b.

The adsorption capacity of MB increases from 3 to 7 and changes slightly when solution pH exceeds 7. When pH < pH_{PZC}, the surface charge is positive,

(CC) 2023 SCS.

and when pH > pH_{PZC}, the surface charge is negative. The pH_{PZC} of CMC is approximately 6.32 (Fig. S-4).

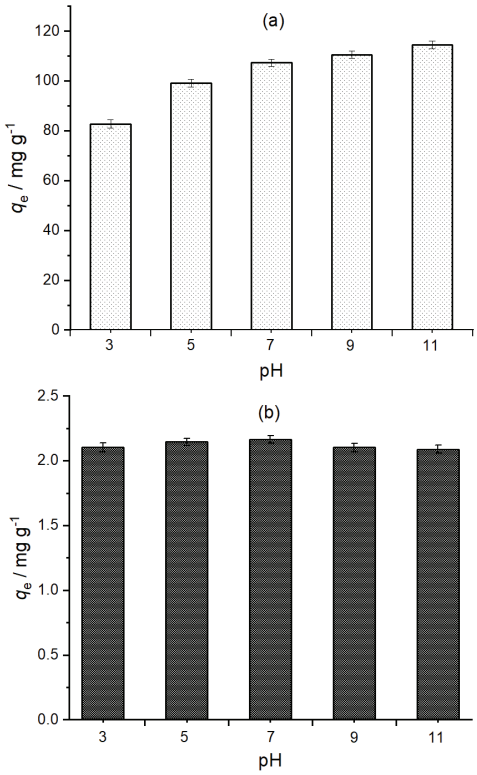

Fig. 3. Influence of pH value on the adsorption of: a) MB and b) As(V).

At low pH, low adsorption capacity resulted from electrostatic repulsion between the cationic ion MB and positively charged active sites on CMC. Electrostatic attraction occurs between negatively active sites on CMC and the cationic ion MB at higher pH levels, facilitating adsorption capacity. Arsenic acid exists in anionic forms ($H_2AsO_4^-$, $HAsO_4^{2-}$, AsO_4^{3-}).[26] Moreover, CMC with positively charged active sites can attract arsenate ions, increasing adsorption capacity from 84.12 to 86.6 %. In contrast, at pH ranging 7 to 11, CMC with negatively charged active sites inhibited As(V) adsorption due to OH^- competing with arsenates, resulting in a decrease in yield to 83.54 %.[27] Hence, the initial pH solution for the following experiments is 7.

Adsorption thermodynamics

A linear van't Hoff plot (Fig. 4a and b) of ln K_D *versus* 1/T gives slope and intercept to determine the value of $\Delta H°$ and $\Delta S°$, respectively. The calculated

(CC) 2023 SCS.

thermodynamic parameters for MB and As(V) adsorption onto CMC are summarized in Table I at different temperatures. As temperature rises, the value of $\Delta G°$ becomes more negative, resulting in more spontaneous adsorption with high affinity of MB and As(V) to CMC. The value of $\Delta H°$ for absolute physical adsorption is typically less than 20 kJ mol^{-1}, whereas chemisorption is in the range of 80 to 200 kJ mol^{-1}.[28,29]

$\Delta H°$ of MB on CMC is 15.06 kJ mol^{-1} indicates physical adsorption while the value of $\Delta H°$ (22.32 kJ mol^{-1}) for As(V) on CMC should be regarded as a mixture of physical adsorption and chemisorption, but dominated by physical adsorption, since the $\Delta H°$ was a slightly higher than 20 kJ mol^{-1}. With positive values of $\Delta S°$, there is an affinity adsorbent for adsorbate.

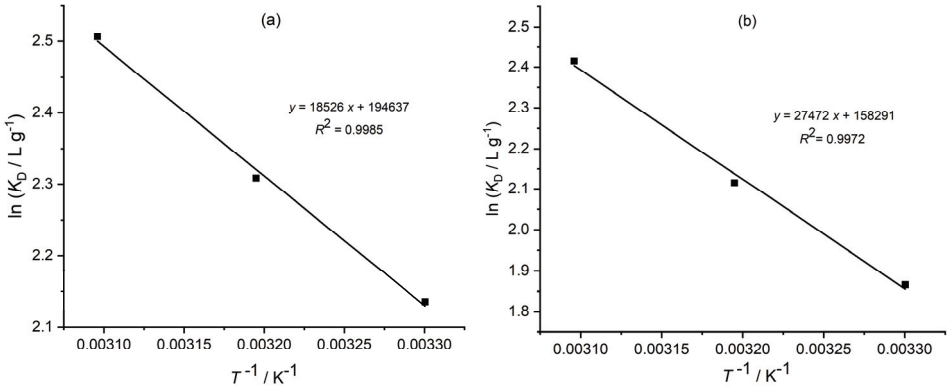

Fig. 4. The plot of ln K_D *vs.* 1/T for: a) MB and b) As(V) adsorption onto CMC.

TABLE I. Thermodynamic parameters for adsorption of adsorbates onto CMC

Adsorbate	Temperature, K	$\Delta S°$ / J mol^{-1} K^{-1}	$\Delta H°$ / kJ mol^{-1}	$\Delta G°$ / kJ mol^{-1}
MB	303	67.41	15.06	–5.38
	313			–6.01
	323			–6.73
As	303	89.10	22.32	–4.70
	313			–5.51
	323			–6.49

Effect of contact time and adsorption kinetics

For both MB and As(V), contact intervals of 0 to 105 min and 0 to 120 min are used to evaluate the adsorption process as a function of contact time, respectively. The adsorption of MB and As(V) occurs in three stages. Firstly, the adsorption rate for MB increases significantly in 10 and 30 min for As(V). The reason for this is that at the start, many vacant sites are available for adsorption. Then, it will gradually rise until it reaches the equilibrium value of 30 min for

(CC) 2023 SCS.

MB and 75 min for As(V) (Fig. 5a and b), resulting from the fewer vacant sites and repulsive forces between the occupied sites and bulk phases.

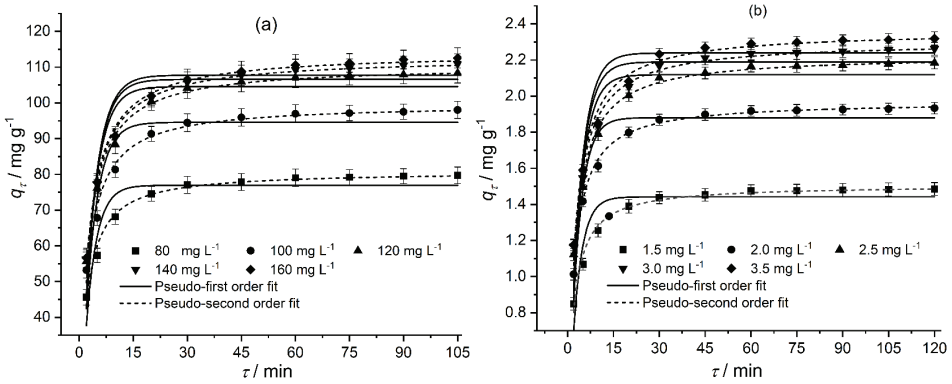

Fig. 5. Kinetic modeling for adsorption of: a) MB and b) As(V) onto CMC.

Therefore, we determined that the adsorption time for the next experiment will be 60 min for MB and 90 min for As(V). Adsorption of MB on the surface of CMC is physical, whereas adsorption of As(V) is both physical and chemical process, resulting in As(V) adsorption being slower than that of MB.[30,31]

To investigate the experimental data, different kinetic models including pseudo-first-order and pseudo-second-order were used to understand the adsorption process. The kinetic parameters, correlation coefficient (R^2) and non-linear chi-square (χ^2) were listed in Table II.

TABLE II. Kinetic parameters for adsorption of a) MB; b) As(V) onto CMC at 303 K

Adsorbate	C_0 mg L^{-1}	First-order kinetic model					Second-order kinetic model			
		$q_{e,exp}$ mg g^{-1}	k_1 min^{-1}	$q_{e,cal}$ mg g^{-1}	R^2	χ^2	k_2 g mg^{-1} min^{-1}	$q_{e,cal}$ mg g^{-1}	R^2	χ^2
MB	80	79.74	0.3357	76.94	0.864	3.043	0.0071	80.87	0.987	0.274
	100	98.03	0.2972	94.56	0.875	4.403	0.0050	99.72	0.986	0.459
	120	108.35	0.2870	104.55	0.900	3.950	0.0042	110.51	0.994	0.207
	140	110.91	0.2830	106.58	0.899	4.120	0.0041	112.78	0.995	0.193
	160	112.57	0.2796	107.75	0.893	4.473	0.0039	114.12	0.994	0.244
As(V)	1.5	1.482	0.3325	1.442	0.867	0.059	0.3774	1.507	0.987	0.006
	2.0	1.929	0.3084	1.880	0.915	0.053	0.2608	1.971	0.998	0.001
	2.5	2.179	0.2784	2.119	0.902	0.089	0.2049	2.227	0.993	0.006
	3.0	2.257	0.2752	2.189	0.888	0.104	0.1961	2.302	0.991	0.009
	3.5	2.312	0.2713	2.239	0.886	0.108	0.1855	2.362	0.989	0.010

The calculated q_e values ($q_{e,cal}$) of both models are comparable to the experimental ones ($q_{e,exp}$). However, the R^2 of the pseudo-second-order kinetic model (approximately 0.99 for R^2) is significantly higher than that of pseudo-

(CC) 2023 SCS.

-first-order kinetic model (approximately 0.90 for R^2), conversely, (χ^2) of the pseudo-second-order kinetic model is significantly lower than that of pseudo-first-order kinetic model, implying that the pseudo-second-order kinetic model is better for adsorption kinetics of MB and As(V) onto CMC.

Effect of initial concentration and adsorption isotherms

Fig. 6a and b indicated that the adsorption capacity of MB and As(V) onto CMC significantly increases with increasing ranges of 80 to 120 mg L^{-1} and 1.5 to 2.5 mg L^{-1}, respectively. When the concentrations of MB and As(V) exceed 120 and 2.5 mg L^{-1}, the adsorption capacity increases insignificantly and reaches a maximum of 110.63 mg L^{-1} (C_0 = 160 mg L^{-1}) and 2.312 mg L^{-1} (C_0 = 3.5 mg L^{-1}), respectively. We can assume three main reasons to explain this phenomenon: 1) a large number of available active sites are used at higher concentrations of MB and As(V), 2) improved mass transfer and 3) the increased ability of MB and As(V) to collide with CMC.

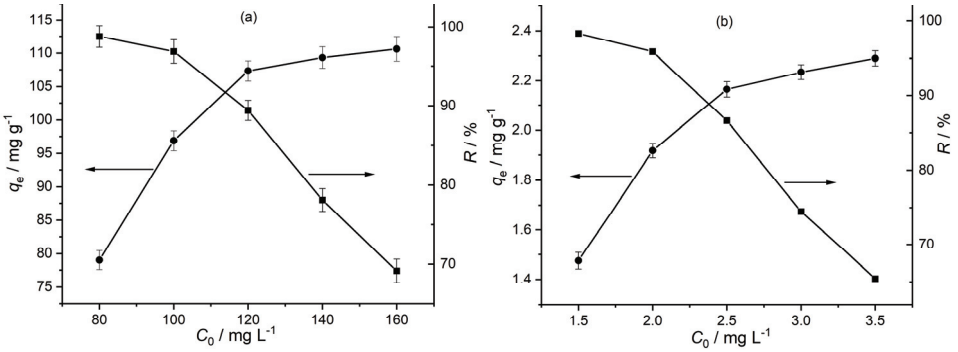

Fig. 6. Effect of initial concentration on adsorption capacity and removal efficiency of a) MB and b) As(V) onto CMC.

Furthermore, as the initial concentration increases from 80 to 160 mg L^{-1} and from 1.5 to 3.5 mg L^{-1}, the removal of MB and As(V) decreases from 98.79 to 69.14 % and from 98.60 to 65.97 %, respectively. When using higher concentrations of adsorbates with the same weight of CMC, the percentage removal of MB and As(V) is reduced because the number of active sites on CMC remains constant.

The Langmuir and Freundlich equations are the most used isotherms equation for modelling the adsorption data. The R^2 obtained from Langmuir model is significantly higher than that obtained from Freundlich model, indicating that the Langmuir isotherm better fits the experimental data (Fig. 7a and b, Table III). Table S-IV compares the adsorption capacity of CMC with various adsorbents. The previously reported capacity of MB and As(V) onto CMC is greater than that

(CC) 2023 SCS.

of many other previously reported adsorbents, implying that the as-prepared CMC has a high potential for use in wastewater treatment. A high K_L value indicates the high affinity of adsorbent for MB and As(V) adsorption.[32,33] The R_L values in the range of 0 and 1 indicate favourable adsorption.

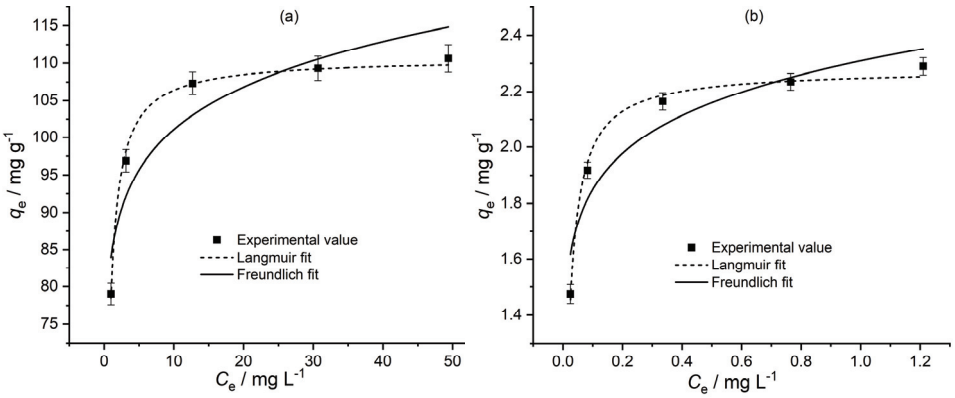

Fig. 7. Analyses of adsorption isotherm for: a) MB and b) As(V) onto CMC by Langmuir and Freundlich models at 303 K.

TABLE III. Isotherm parameters for adsorption of MB and As(V) onto CMC at different concentration

Adsorbate	$q_{e,exp}$ mg g^{-1}	Langmuir isotherm model					Freundlich isotherm model			
		q_{max} mg g^{-1}	K_L L mg^{-1}	R_L	R^2	χ^2	K_F mg g (L/ mg)$^{1/n}$	n_F	R^2	χ^2
MB	110.63	110.64	2.518	0.003	0.996	0.027	84.138	12.546	0.884	24.427
As(V)	2.31	2.285	81.919	0.003	0.985	0.003	2.325	10.950	0.904	0.608

Reusability

CMC regeneration and recycling are critical for practical application. As shown in Fig. 8a and b, after five cycles, there is only a very slight decrease in

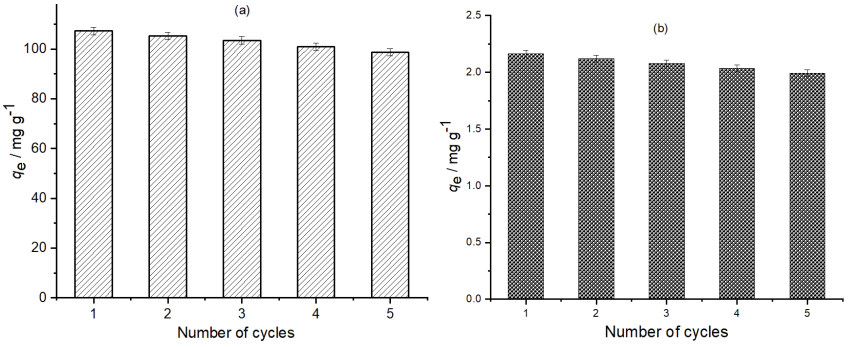

Fig. 8. Regeneration for: a) MB and b) As(V) adsorption onto CMC.

(CC) 2023 SCS.

removal from 107.32 to 98.73 mg g^{-1} for MB and from 2.165 to 1.992 mg g^{-1} for As(V), indicating that CMC has excellent performance and application for MB and As (V) treatment.

CONCLUSION

CMC was prepared in a straightforward and efficient manner. They also have a fast adsorption rate, high adsorption efficiency, and fast magnetic separation from treated water, making them excellent materials for environmentally friendly water treatment. The maximum adsorption is 110.63 mg g^{-1} for MB and 2.31 mg g^{-1} for As(V). The kinetics of adsorption can be described using a pseudo-second-order equation, and the CMC adsorption isotherm agreed well with the Langmuir sorption equation. Furthermore, through the desorption process the product could be regenerated and reused multiple times.

SUPPLEMENTARY MATERIAL

Additional data and information are available electronically at the pages of journal website: https://www.shd-pub.org.rs/index.php/JSCS/article/view/12026, or from the corresponding author on request.

ИЗВОД

КАРАКТЕРИЗАЦИЈА МАГНЕТНОГ НАНОКОМПОЗИТА ПРЕВУЧЕНОГ УГЉЕНИКОМ ЗА УКЛАЊАЊЕ МЕТИЛЕНСКОГ ПЛАВОГ И АРСЕНАТА ИЗ ВОДЕНОГ РАСТВОРА

NGOC BICH NGUYEN[1,2], THI QUE PHUONG PHAN[3], CAO THANH TUNG PHAM[1,4], HUU NGHI NGUYEN[2], SY NGUYEN PHAM[5] и DINH THANH NGUYEN[1,3]

[1]Graduate University of Science and Technology, Viet Nam Academy of Science and Technology, Hanoi City, 100000, Vietnam, [2]Dong Thap University, Cao Lanh City, 870000, Vietnam, [3]Institute of Applied Materials Science, Viet Nam Academy of Science and Technology, Ho Chi Minh City, 700000, Vietnam, [4]Institute of Chemical Technology, Viet Nam Academy of Science and Technology, Ho Chi Minh City, 700000, Vietnam и [5]Ho Chi Minh City University of Natural Resources and Environment, Vietnam

Магнетни нанокомпозит превучен угљеником произведен ниско-температурском хидротермалном методом је употребљен за уклањање метиленског плавог и арсената из воденог раствора. Лангмиров модел је добро описао експерименталне податке са израчунатим максималним адсорпционом капацитетом од 110,63 и 2,31 mg g^{-1} за метиленско плаво и арсенат, редом. Такође, одређени адсорпциони механизми су физисорпција за метиленско плаво и комбинација физисорпције и хемисорпције за арсенат. Промена Гибсове енергије има негативне вредности што указује на то да се адсорпција метиленско плавог и арсената на магнетним материјалима дешава спонтано. Ово истраживање показује једноставну, ефикасну и поуздану методу за уклањање метиленско плавог и арсената.

(Примљено 2. августа, ревидирано 5. октобра, прихваћено 3. новембра 2022)

REFERENCES

1. S. Ji, C. Miao, H. Liu, L. Feng, X. Yang, H. Guo, *Nanoscale Res. Lett.* **13** (2018) 178 (https://doi.org/10.1186/s11671-018-2580-8)
2. W. J. Liu, K. Tian, H. Jiang, H. Q. Yu, *Sci Rep* **3** (2013) 2419 (https://doi.org/10.1080/19443994.2015.1132476)

(CC) 2023 SCS.

3. T. H. Nguyen, T. H. Pham, H. T. N. Thi, T. N. Nguyen, M. V. Nguyen, T. T. Dinh, M. P. Nguyen, T. Q. Do, T. Phuong, T. T. Hoang, T. T. M. Hung, V. H. T. Thi, *J. Chem.* **2019** (2019) 1 (https://doi.org/10.1155/2019/5295610)
4. M. Inyang, B. Gao, P. Pullammanappallil, W. Ding, A. R. Zimmerman, *Bioresour. Technol.* **101** (2010) 8868 (https://doi.org/10.1016/j.biortech.2010.06.088)
5. N. Besharati, N. Alizadeh, S. Shariati, *J. Mex. Chem. Soc.* **62** (2018) 110 (https://doi.org/10.29356/jmcs.v62i3.433)
6. W. Chen, R. Parette, J. Zou, F. Cannon, B. Dempsey, *Water Res.* **41** (2007) 1851 (https://doi.org/10.1016/j.watres.2007.01.052)
7. M. Zhang, B. Gao, S. Varnoosfaderani, A. Hebard, Y. Yao, M. Inyang, *Bioresour. Technol.* **130** (2013) 457 (https://doi.org/10.1016/j.biortech.2012.11.132)
8. L. Huang, J. Cai, M. He, B. Chen, B. Hu, *Ind. Eng. Chem. Res.* **57** (2018) 6201 (https://doi.org/10.1021/acs.iecr.7b05294)
9. N. S. Pham, P. T. Q. Phan, B. N. Nguyen, V. X. Le, *J. Appl. Electrochem.* (2022) (https://doi.org/10.1007/s10800-022-01747-1)
10. N. S. Pham, V. X. Le, *J. Electroanal. Chem.* **921** (2022) 116507 (https://doi.org/10.1016/j.jelechem.2022.116507)
11. N. S. Pham, B. N. Nguyen, A. Q. K. Nguyen, *J. Appl. Electrochem.* (2022) (https://doi.org/10.1007/s10800-022-01784-w)
12. K. Dai, F. Wang, W. Jiang, Y. Chen, J. Mao, J. Bao, *Nanoscale Res. Lett.* **12** (2017) 528 (https://doi.org/10.1186/s11671-017-2295-2)
13. N. S. Pham, Y. H. Seo, E. Park, T. D. D. Nguyen, I.-S. Shin, *Data Br.* **31** (2020) 105891 (https://doi.org/10.1016/j.dib.2020.105891)
14. N. S. Pham, Y. H. Seo, E. Park, T. D. D. Nguyen, I.-S. Shin, *Electrochim. Acta* **353** (2020) 136446 (https://doi.org/10.1016/j.electacta.2020.136446)
15. V. X. Le, H. Lee, N. S. Pham, S. Bong, H. Oh, S.-H. Cho, I.-S. Shin, *Sensors Actuators, B* **346** (2021) 130552 (https://doi.org/10.1016/j.snb.2021.130552)
16. N. S. Pham, P. T. Q. Phan, V. X. Le, *J. Appl. Electrochem.* **52** (2022) 1343 (https://doi.org/10.1007/s10800-022-01716-8)
17. L. Zhu, F. Shen, R. L. Smith, L. Yan, L. Li, X. Qi, *Chem. Eng. J.* **316** (2017) 770 (https://doi.org/10.1016/j.cej.2017.02.034)
18. L. Ai, C. Zhang, Z. Chen, *J. Hazard Mater.* **192** (2011) 1515 (https://doi.org/10.1016/j.jhazmat.2011.10.041)
19. X. Bao, Z. Qiang, J.-H. Chang, W. Ben, J. Qu, *J. Environ. Sci.* **26** (2014) 962 (https://doi.org/10.1016/S1001-0742(13)60485-4)
20. L. Verma, M. A. Siddique, J. Singh, R. N. Bharagava, *J. Environ. Manage.* **250** (2019) 109452 (https://doi.org/10.1016/j.jenvman.2019.109452)
21. J. Wang, J. Xu, N. Wu, *J. Exp. Nanosci.* **12** (2017) 297 (https://doi.org/10.1080/17458080.2017.1325016)
22. B. Qiu, H. Gu, X. Yan, J. Guo, Y. Wang, D. Sun, Q. Wang, M. Khan, X. Zhang, B. L. Weeks, D. P. Young, Z. Guo, S. Wei, *J. Mater. Chem. A* **2** (2014) 17454 (https://doi.org/10.1039/C4TA04040F)
23. H. Zeng, W. Qi, L. Zhai, F. Wang, J. Zhang, D. Li, *J. Environ. Chem. Eng.* **9** (2021) 105951 (https://doi.org/10.1016/j.jece.2021.105951)
24. Y. Bulut, H. Aydın, *Desalination* **194** (2006) 259 (https://doi.org/10.1016/j.desal.2005.10.032)
25. K. Y. Foo, B. H. Hameed, *Desalin. Water Treat.* **19** (2012) 255 (https://doi.org/10.5004/dwt.2010.1214)

(CC) 2023 SCS.

26. A. Sharma, N. Verma, A. Sharma, D. Deva, N. Sankararamakrishnan, *Chem. Eng. Sci.* **65** (2010) 3591 (https://doi.org/10.1016/j.ces.2010.02.052)
27. X. Shi, C. Wang, Y. Ma, H. Liu, S. Wu, Q. Shao, Z. He, L. Guo, T. Ding, Z. Guo, *Powder Technol.* **356** (2019) 726 (https://doi.org/10.1016/j.powtec.2019.09.002)
28. B. Gu, J. Schmitt, Z. Chen, L. Llang, J. F. McCarthy, *Environ. Sci. Technol* **28** (1994) 38 (https://doi.org/10.1021/es00050a007)
29. L. Ding, B. Zou, W. Gao, Q. Liu, Z. Wang, Y. Guo, X. Wang, Y. Liu, *Colloids Surfaces, A* **446** (2014) 1 (https://doi.org/10.1016/j.colsurfa.2014.01.030)
30. C. Li, Z. Xiong, J. Zhang, C. Wu, *J. Chem. Eng. Data* **60** (2015) 3414 (https://doi.org/10.1021/acs.jced.5b00692)
31. T. S. Anirudhan, J. Nima, S. Sandeep, V. R. N. Ratheesh, *Chem. Eng. J.* **209** (2012) 362 (https://doi.org/10.1016/j.cej.2012.07.129)
32. M. A. Ahmad, N. A. Ahmad Puad, O. S. Bello, *Water Resour. Ind.* **6** (2014) 18 (https://doi.org/10.1016/j.wri.2014.06.002)
33. X. Zhou, J. Zhou, Y. Liu, J. Guo, J. Ren, F. Zhou, *Fuel* **233** (2018) 469 (https://doi.org/10.1016/j.fuel.2018.06.075).

(CC) 2023 SCS.